Journal of the Optical Society of America B
OPTICAL PHYSICS

Compact and efficient 2D and 3D designs for photonic-to-plasmonic coupler

KHALED S. R. ATIA,[1] AFAF SAID,[2] AHMED HEIKAL,[3] AND S. S. A. OBAYYA[2,*]

[1]Advanced Research Complex, University of Ottawa, Ottawa, ON K1N 6N5, Canada
[2]Center for Photonics and Smart Materials, Zewail City of Science and Technology, Giza 12578, Egypt
[3]Faculty of Engineering, Mansoura University, Mansoura 35516, Egypt
*Corresponding author: sobayya@zewailcity.edu.eg

Received 12 February 2019; revised 8 April 2019; accepted 11 April 2019; posted 12 April 2019 (Doc. ID 360044); published 7 May 2019

Two ultra-compact designs of wideband photonic to metal-dielectric-metal (MDM) couplers are introduced. The two proposed couplers show a high efficiency of 92% and 94% at unexpected very small coupling lengths, using MDM as a coupling waveguide. Emerging from the half-wavelength transformer concept, when the characteristic impedances of the coupled waveguides are equal in magnitude but have a phase difference, we report a slight shift in the coupler length of the first maximum. Relying on this concept, the lengths of the proposed couplers are 10 nm and 15 nm, respectively, to match the phase shift. The proposed couplers also enjoy a very wide bandwidth of 1785 nm for the 10 nm design and 1865 nm for the 15 nm design because of the short coupling length. Also, we introduce a 3D design for the coupler based on a quasi-MDM waveguide of a 20 nm silver layer to facilitate the fabrication process. The simulation results are produced by 2D finite element methods and verified by 3D finite difference time domain, but with incomparable computational cost.

https://doi.org/10.1364/JOSAB.36.001402

1. INTRODUCTION

Over the last decade, plasmonics has received an increased interest due to its well-known strength in concentrating light to the nanoscale and producing high local-field confinement beyond the diffraction limit [1]. Such ability has inspired researchers to further break the limit of data communication by introducing plasmonic waveguides as optical interconnects to high-speed transistors [2]. Particularly, metal-dielectric-metal (MDM) waveguides can have propagating modes over a wide band of frequencies that extends from DC to visible [3]. Recently, MDM waveguides have been used in several applications, including sensing [4], filtering [5], energy harvesting [6], and wavelength division multiplexing [7]. However, metallic losses in plasmonic waveguides limit the data transmission over long distances. Therefore, a solution would be utilizing a conventional waveguide for longer distances. This solution requires designing an efficient broadband photonic-to-plasmonic coupler.

One way to design an efficient plasmonic coupler is by using corrugated tapers. Since the conductivity of most metals is very high, regular surface plasmon polaritons are very poorly confined to metal-dielectric interface, whereas corrugation of the metal surface permits the confinement of spoof surface plasmon waves. Based on this idea, a coupling efficiency of 72% was achieved from a 6.2-μm-wide input opening into a 20 nm gap width [8]. Also, an outstanding insertion loss of 2 dB has been attained for a 300 nm gap width with a total 3.15 μm coupler length. However, the phase between two adjacent groves in the corrugation has to be preserved, which means the incident lights falling on each groove should be in phase for higher coupling efficiency. These conditions constrain the coupler design efficiency and size. An alternative approach was based on "partially" corrugated tapers [9], where a closed structure is used instead of an open structure. Using this approach, a 98% coupling efficiency with a 1.5 μm total coupling length has been achieved. However, the gap size of the MDM waveguide is 300 nm. Another way is to use optimized multi-section tapers [10]. The multi-section tapers structure has shown a high efficiency (93%) and coupling length (400 nm) when used in coupling between 300 nm silicon waveguide and 50 nm MDM waveguide. The basic idea is to design sections capable of reducing the impedance mismatch between a silicon waveguide and plasmonic waveguide. However, the complicity of such multi-section based coupler makes its fabrication very difficult. It was also found that the coupling efficiency can be improved by preventing transverse "funnel leakage" at the interface between the dielectric waveguide and the plasmonic waveguide [11]. Based on this idea, only an 88% coupling efficiency was achieved by inserting a 33-nm-long rectangular air-gap between the 300 nm silicon waveguide and 40 nm plasmonic waveguide [12].

The behavior of MDM waveguides has been accurately described through a characteristic impedance model [13]. This model has also been used to couple MDM waveguides

of different gap widths via a quarter-wavelength transformer [14]. However, this model cannot predict the impedance of the coupler between photonic and plasmonic waveguides due to the radiation losses that arise from direct coupling and the lack of an accurate photonic waveguide characteristic impedance model. Recently, an analytical model was developed to predict the transmission characteristics of silicon to plasmonic couplers [15]. The developed model relies on the boundary conditions and the mode-matching technique to describe the behavior of the butt coupling. Although accurate, it is not able to predict a matching coupler.

Our contribution in this paper may be summarized as the following: we introduce silicon-to-plasmonic coupler designs with an ultra-compact coupling length (10 nm) up to 40 times smaller than the coupler reported in the literature [10] achieving almost the same high efficiency (93%). A high efficiency up to 94% is obtained, and a broad bandwidth of 1865 nm is achieved, which is, to the best of our knowledge, the highest bandwidth so far. We introduce the modified principle of half-wavelength transformer that could accurately predict this unexpected small coupling length. In addition, the simulation results of the designs proposed are investigated using the accurate and fast bidirectional beam propagation method (BIBPM) [16], which show very good prediction for the 3D structure using a finite difference time domain (FDTD), but with incomparable computational cost. Moreover, to avoid the difficulties of MDM fabrication [10,17], we introduce a 3D design for the coupler based on quasi-MDM waveguide with a thin layer (20 nm) of silver to make use of the skin effect of metals.

2. MATHEMATICAL FORMULATION FOR 2D ANALYSIS

Since the beam propagation method (BPM) is known for its simplicity and speed, BPMs based on the iterative methods such as Taylor and Padé approximations [16] are frequently used in a photonic devices analysis to calculate the square root operators representing each waveguide. However, they show huge failure while dealing with such challenging high-index-contrast structures like in this coupler [16] because of their disability to correctly model the evanescent modes in the square root operators. Moreover, for a high numerical precision, the Blocked Schur (BS) algorithm is faster, especially for accurate treatment of surface plasmon polaritons (SPPs) [16]. Therefore, we adopt here the efficient and fast Blocked Schur-finite element-bidirectional beam propagation method (BS-FE-BiBPM) [16], which is more efficient, while dealing with the surface, evanescent, and even nonphysical modes to accurately characterize the proposed coupler shown in Fig. 1(b). The Schur decomposition,

$$[A] = [Q][T][Q^*], \tag{1}$$

represents all the eigenvalues of the characteristic matrix $[A]$ in the diagonal of the triangular matrix $[T]$.

Each waveguide i in the coupler could be governed by a 2D Helmholtz equation. First, we divided the transverse direction, y, into a number of first-order linear elements using the standard Galerkin's finite element procedure. Then, we treated the

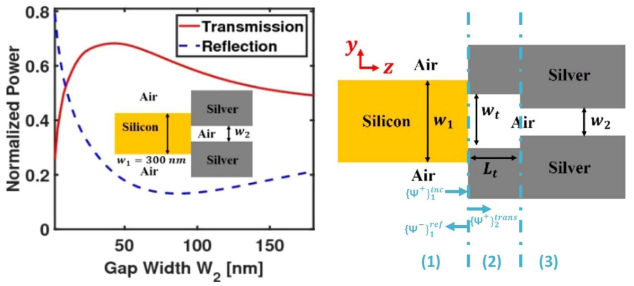

Fig. 1. (a) Transmission and reflection of a 300 nm silicon waveguide butt coupled to an MDM waveguide of a changing gap width W_2 from 10 nm to 180 nm. (b) Proposed coupler between a silicon waveguide and an MDM waveguide. W_t is the width of the coupler, and L_t is the length of the coupler.

multiple discontinuities in the propagation direction, z, by adopting the BS-FE-BiBPM [16] to calculate the transmission and reflection. The accurate calculation for the square root operators is very important to employing the continuity of the transverse magnetic and electric fields at each transition steps between waveguides i and $i+1$:

$$2[P]_i\sqrt{[A]_i}\{\psi^+\}_i^{\text{inc}} = \left([P]_i\sqrt{[A]_i} + [P]_{i+1}\sqrt{[A]_{i+1}}\right)\{\psi^+\}_{i+1}^{\text{trans}}, \tag{2}$$

$$\left([P]_i\sqrt{[A]_i} - [P]_{i+1}\sqrt{[A]_{i+1}}\right)\{\psi^+\}_i^{\text{inc}} = \left([P]_i\sqrt{[A]_i} + [P]_{i+1}\sqrt{[A]_{i+1}}\right)\{\psi^-\}_i^{\text{ref}}, \tag{3}$$

and to propagation steps,

$$\{\psi\}_i(z) = \exp\left(+j\sqrt{[A]_i}z\right)\{\psi^+\}_i + \exp\left(-j\sqrt{[A]_i}z\right)\{\psi^-\}_i, \tag{4}$$

where $\{\psi^-\}_i$ and $\{\psi^+\}_i$ are the backward and forward propagating fields, respectively, in the i-th waveguide, and $\{\psi^+\}_i^{\text{inc}}$, $\{\psi^+\}_{i+1}^{\text{trans}}$, and $\{\psi^-\}_i^{\text{ref}}$ are incident, transmitted, and reflected fields, respectively, at each discountinuity plane, as shown in Fig. 1(b). $[P]_i$ is a diagonal matrix function of the relative permittivity for transverse magnetic (TM) SPPs [16]. Also, the smoothed finite elements method [18] is used here to analyze the filed profile of the couplers.

3. DESIGN CRITERIA

Figure 1(a) shows the transmission and reflection of a 300 nm Silicon waveguide butt coupled to a MDM waveguide with a gap width W_2 varying from 10 nm to 180 nm. Such design has been studied in [10]. A maximum coupling efficiency of 68% can be noticed at the gap width of 40 nm. Although a characteristic impedance model for the MDM waveguides has been previously proposed [13], the transmission line model cannot predict the performance of the structure shown in Fig. 1(a) due to the ambiguity of the characteristic impedance of the silicon waveguide. Moreover, there are radiation modes arising from the direct coupling [16]. Based on the MDM impedance model, a quarter-wavelength transformer has been introduced

to couple two MDM waveguides of different gap widths [14], where the characteristic impedance of the transformer equals the square root of the product of the two waveguides impedance, and the length satisfies odd multiples of quarter wavelength [19]. Although this model cannot be applied here to predict the dimensions of the transformer, the concept of matching using a transformer is still valid. Therefore, we propose the structure shown in Fig. 1(b), and the dimensions of the matching waveguide are investigated numerically.

A. Finding Minimum Radiation Losses

An MDM waveguide is chosen for matching to limit the sources of radiation modes. Since we seek a highly efficient coupling, it is required first to reduce the SPPs generated between the silicon and the MDM waveguide that cause radiation losses. Therefore, the variation of the radiation losses for different MDM gap widths is studied in Fig. 2. In the design process, the propagation length inside the MDM narrow gap W_2 should be taken into consideration, since narrower gaps have smaller propagation lengths. Therefore, $W_2 = 40$ nm is chosen as the lower limit of the study. It may be observed that the radiation losses decrease with the increase of W_1. Also, starting from $W_1 = 400$ nm to $W_1 = 500$ nm, the radiation losses vary slightly, especially for $W_2 = 40$ nm and 50 nm. Therefore, we propose two different designs than the one reported in [10]. The first proposed design has a silicon waveguide width of 400 nm and an MDM gap of 40 nm. The second suggested design has a 400 nm silicon waveguide width and an MDM gap of 50 nm. Table 1 shows the transmission, reflection, and radiation losses at 1550 nm for the two proposed structures compared to the dimensions reported previously in [10]. This can be attributed to the leakage of the SPPs generated at the interface.

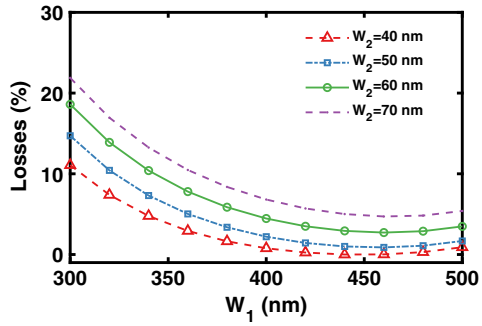

Fig. 2. Sweep simulation to find the minimum radiation losses.

Table 1. Transmission (T), Reflection (R), and Radiation Losses (R.L) Comparison between the Two Proposed Couplers and the Direct Coupling Structure as Reported in [10]

	Literature [10]	First Design	Second Design
W_1	300 nm	400 nm	400 nm
W_2	40 nm	40 nm	50 nm
T	68%	53%	56%
R	21%	46%	42%
R.L	11%	0%	2%

Although these dimensions reduce the radiation losses, the transmission efficiency has been severely reduced. The degradation in the transmission efficiency is then handled by the proposed transformer.

B. Modifying $\lambda/2$ Transformer

We study the transmission efficiency of the first set of dimensions after introducing a matching MDM waveguide between the silicon waveguide ($W_1 = 400$ nm) and the plasmonic waveguide ($W_2 = 40$ nm). Figure 3(a) shows the variation of the transmission efficiency with the length of the matching MDM waveguide for different matching MDM gap widths of 200 nm, 240 nm, 290 nm, and 340 nm. The maximum transmission achieved is 92% and is obtained at the dimensions $W_t = 240$ nm and $L_t = 10$ nm. Moreover, the inset of Fig. 3(a) indicates very good fabrication tolerances for this design, which means that characteristics impedance of the coupler is arbitrary for the four simulated gap widths. This can be conceptually explained by the following relation that describes the reflection from a single slab between two different mediums:

$$R = \frac{\rho_1 + \rho_2 e^{-2jk_t L_t}}{1 + \rho_1 \rho_2 e^{-2jk_t L_t}}, \tag{5}$$

where L_t is the thickness of the slab, k_t is the wave number inside the slab, and ρ_1 and ρ_2 represent the reflection from the first and the second interfaces, respectively. In order for the reflection to be zero, the following condition has to be satisfied:

$$-\rho_1 = \rho_2 e^{-2jk_t L_t}. \tag{6}$$

However, the complex nature of the cavity and the plasmonic waveguide introduces additional phases θ_1 and θ_2 to ρ_1 and ρ_2, respectively. Also, an additional phase Φ_{SPP} is presented due to the coupled SPPs. Hence, Eq. (6) can be rewritten as

$$-\rho_1 = \rho_2 e^{-j(2k_t L_t + \theta_2 - \theta_1 + \Phi_{SPP})}. \tag{7}$$

By assuming that the imaginary parts of k_t and L_t are small, the condition that makes the choice of z_t arbitrary is $\rho_1 = -\rho_2$ [20,21], which explains the slight differences in transmission between different gap sizes of the coupler. Under this condition,

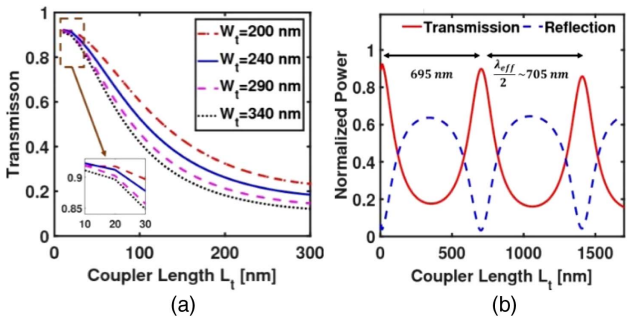

Fig. 3. Variation of the transmission efficiency of the first dimensions ($W_1 = 400$ nm and $W_2 = 40$ nm) with the coupler length L_t computed for different MDM coupler widths ($W_t = 40$ nm, 240 nm, 290 nm, and 340 nm). (b) The variation of the transmission and reflection as a function of the coupling length for a 400 nm silicon waveguide coupled with a 40 nm MDM waveguide using an MDM waveguide of a width $W_t = 240$ nm and length L_t.

the exponential term has to equal 1, which leads to the following condition for the coupler length:

$$L_t = \left(\frac{n}{2} - \frac{\theta_2 - \theta_1 + \Phi_{SPP}}{4\pi}\right)\lambda_{eff}, \qquad n = 0, 1, 2, \ldots, \quad (8)$$

where λ_{eff} is the effective wavelength. Since L_t has to be small in order for $\rho_1 = -\rho_2$ to hold, Eq. (8) is limited to the first maximum ($n = 0$) only. Therefore, the first peak appears at $L_t = (\theta_1 - \theta_2 + \Phi_{SPP})\lambda_{eff}/4\pi$ instead of $L_t = 0$ in normal case where no phase difference exists.

4. SIMULATION RESULTS

A. 10 nm Coupler Design

Figure 4 shows the profile of the magnetic field $|H_x|$ for the coupler at two different coupling lengths $L_t = 10$ nm and $L_t = 705$ nm, respectively. The power is incident from the silicon waveguide, and slight ripples can be noticed in the silicon waveguide due to the interference between the incident wave and the reflected one. Further, the performance of the coupler at the coupling length $L_t = 10$ nm and $L_t = 705$ nm with the wavelength is investigated in Fig. 5. It may be observed that the coupler with $L_t = 10$ nm is almost immune to the change in

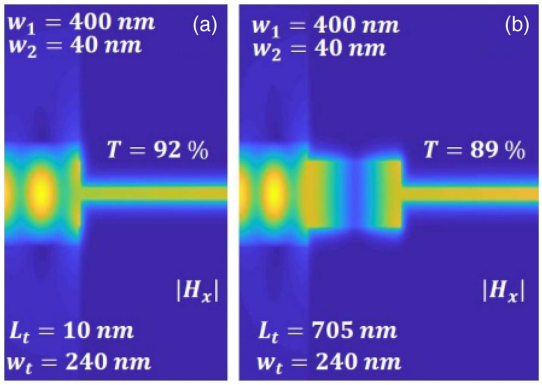

Fig. 4. Field profile of $|H_x|$ of a silicon waveguide of width $W_1 = 400$ nm coupled to a plasmonic waveguide of gap width $W_2 = 40$ nm using (a) an MDM waveguide of length $L_t = 10$ nm and width $W_t = 240$ nm and (b) an MDM waveguide of length $L_t = 705$ nm and width $W_t = 240$ nm.

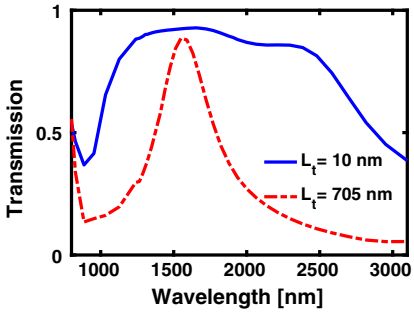

Fig. 5. Variation of the transmission with the wavelength for the proposed coupler of width $W_t = 240$ nm and two coupling lengths $L_t = 10$ nm and $L_t = 705$ nm.

wavelength from $\lambda = 1033$ nm to $\lambda = 2818$ nm, which is, to the best of our knowledge, the widest coupler bandwidth reported. Choosing a very small coupling length $L_t = 10$ nm causes the exponential in Eq. (5) to approach unity leaving the transmission constant over a very wide range. On the other hand, for $L_t = 705$ nm, we can see the transmission peaks at 1550 nm providing a narrower bandwidth from 1378 nm to 1770 nm. At such a long device length, the losses of the metal increase due to the higher dependence of the metal permittivity on the wavelength [12]. The data for silver permittivity are obtained from [22].

B. 15 nm Coupler Design

The transmission is slightly increased to 94% at $W_t = 290$ nm and $L_t = 15$ nm. The width of the plasmonic coupler at which the maximum transmission occurs is different from the first dimension due to the difference in the characteristic impedance between $W_2 = 40$ nm and $W_2 = 50$ nm, as concluded from the model in [13]. The small change in the coupling length is contributed to the change in the characteristic impedance of the matching MDM waveguide, which in turn changes λ_{eff} to 1430 nm. It is also noted from the inset of Fig. 6(a) that the difference in the transmission between the four gap widths is very small as an indication to the arbitrariness of z_t. Figure 6(b) shows the variation of the transmission and the reflection with the coupler length for a coupler of width $W_t = 290$ nm. We see here the periodicity of the transmission where the first peak appears at 15 nm, while the second and third appear at 715 nm and 1430 nm, respectively. The difference between the first two peaks is 700 nm ($\lambda_{eff}/2 - 15$ nm), and the difference between the second two peaks is approximately 715 nm ($\lambda_{eff}/2$). Also, a slight reduction in the transmission between the transmission peaks is a result of plasmonic losses. The transmission equals 0.94, 0.93, and 0.89 for coupler lengths of 15 nm, 715 nm, and 1430 nm, respectively. Figure 7 show the profile $|H_x|$ for the coupler at two different coupling lengths $L_t = 15$ nm and $L_t = 715$ nm, respectively. Furthermore, Fig. 8 shows the variation of the transmission with the wavelength for the two coupling lengths. Similarly, the shorter length $L_t = 15$ nm reveals an immunity to

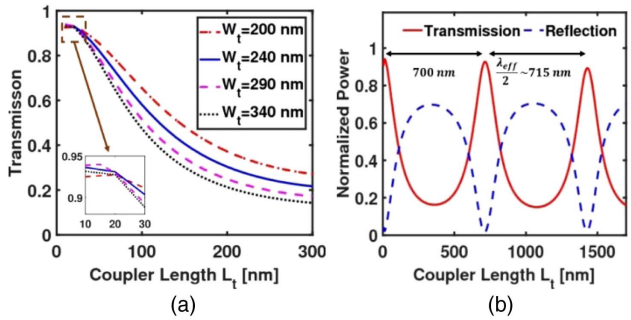

Fig. 6. Variation of the transmission efficiency of the first dimensions ($W_1 = 400$ nm and $W_2 = 50$ nm) with the coupler length L_t computed for different MDM coupler widths ($W_t = 200$ nm, 240 nm, 290 nm, and 340 nm). (b) The variation of the transmission and reflection as a function of the coupling length for a 400 nm silicon waveguide coupled with a 50 nm MDM waveguide using a MDM waveguide of a width $W_t = 290$ nm and length L_t.

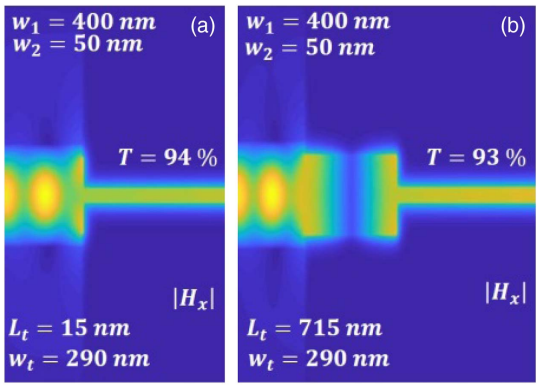

Fig. 7. Field profile of $|H_x|$ of the silicon waveguide of width $W_1 = 400$ nm coupled to a plasmonic waveguide of a gap width $W_2 = 50$ nm using (a) an MDM waveguide of length $L_t = 15$ nm and width $W_t = 290$ nm and (b) an MDM waveguide of length $L_t = 715$ nm and width $W_t = 290$ nm.

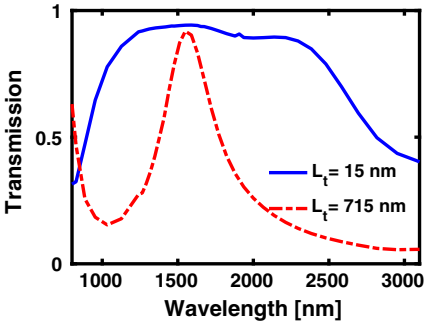

Fig. 8. Variation of the transmission with the wavelength for the proposed coupler of width $W_t = 290$ nm and two coupling lengths $L_t = 15$ nm and $L_t = 715$ nm.

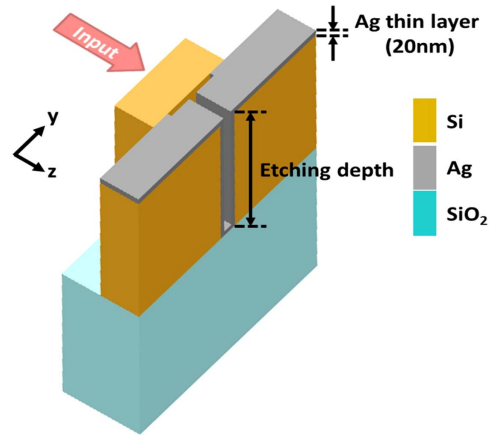

Fig. 9. 3D structure for the first coupler of width $W_t = 240$ nm and coupling length $L_t = 10$ nm using a thin layer (20 nm) of silver on SiO_2 substrate.

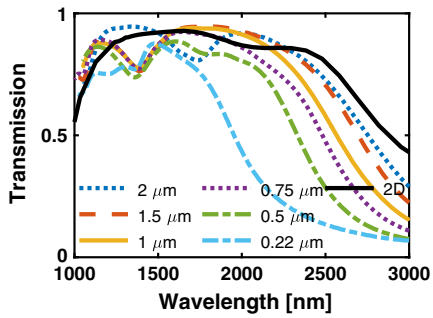

Fig. 10. 3D simulation results of the transmission spectrum while reducing the etching depth from 2 μm to 220 nm for the proposed coupler of width $W_t = 240$ nm and coupling length $L_t = 10$ nm on SiO_2 substrate.

wavelength changes that extends from 953 nm to 2818 nm, while $L_t = 715$ nm peaks near $\lambda = 1550$ nm, presenting a narrower bandwidth from 1409 nm to 1770 nm.

Similarly, a slight enhancement in the transmission efficiency can be obtained when the width of the silicon waveguide is fixed to $W_1 = 400$ nm, and the width of the plasmonic waveguide is $W_2 = 50$ nm. Figure 6(a) shows the variation of the transmission efficiency with the length of the matching MDM waveguide for different matching MDM gap widths of 200 nm, 240 nm, 290 nm, and 340 nm.

C. 3D Coupler Design: Facilitating Fabrication Process

Since creating deep trenches in a bulk metal to produce an MDM waveguide is still a challenging fabrication techniques [17], we converted our 2D coupler design to 3D using a quasi-MDM waveguide with a thin layer (20 nm) of silver, and the skin effect of metals as shown in Fig. 9. The widely employed silicon waveguides in industry have the height value ranging from 220 nm to 500 nm, so the 3D simulation was targeted at this depth range. We used a 3D FDTD to study the effect of changing the etching depth from 2 μm to 220 nm on the transmission spectrum. Figure 10 shows that we got results very similar to those obtained by our 2D simulation tools with incomparable computational cost. However, reducing the etching depths affected the bandwidth to be narrower. At smaller etching depths, the wave guided started to behave as a quasi-TM-like polarization. While considering the etching depth in the 3D simulation, we noticed the silicone waveguide starts to support multi-modes. Since the matching cavity is designed for the fundamental mode, other modes do not couple with similar efficiency. That is why we in Fig. 10 can see a sudden reduction in the transmission shifted toward a higher wavelength at deeper etching depths. In addition, we changed the substrate from silicon to silicon dioxide (SiO_2); however, the results remained almost the same.

5. CONCLUSION

The concept of a half-wavelength transformer has been investigated for the coupling between a photonic waveguide and an MDM plasmonic waveguide. Two different designs for coupling a silicon waveguide to plasmonic waveguide have been introduced. The first design ($W_t = 240$ nm) to couple a

400 nm silicon waveguide anda 40 nm MDM waveguide has shown the shortest coupling length ($L_t = 10$ nm), a high efficiency at 92%, and a wide bandwidth from 1033 nm to 2138 nm. Moreover, the second design ($W_t = 290$ nm) to couple a 400 nm silicon waveguide and a 50 nm MDM waveguide has shown a coupling length of ($L_t = 15$ nm), the highest coupling efficiency at 94%, and a very wide bandwidth from 953 nm to 2138 nm. Moreover, the 3D coupler design proposed based on the quasi-MDM waveguide of a 20 nm silver layer has achieved very good agreement with our 2D results, while avoiding the difficulties of fabricating an MDM waveguide.

Funding. National Telecommunication Regulatory Authority (NTRA), Ministry of Communication and Information Technology.

Acknowledgment. The authors would like to express their gratitude to the National Telecommunication Regulatory Authority, Ministry of Communication and Information Technology in Egypt, for providing the financial support for this research.

REFERENCES

1. M. L. Brongersma, "Introductory lecture: nanoplasmonics," Faraday Discuss. **13**, 1–28 (2015).
2. E. Ozbay, "Plasmonics: merging photonics and electronics at nanoscale dimensions," Science **311**, 189–193 (2006).
3. E. N. Economou, "Surface plasmons in thin films," Phys. Rev. **182**, 539–554 (1969).
4. S. Luo, B. Li, D. Xiong, D. Zuo, and X. Wang, "A high performance plasmonic sensor based on metal-insulator-metal waveguide coupled with a double-cavity structure," Plasmonics **12**, 223–227 (2017).
5. F. Zou, X. Zou, W. Pan, B. Luo, and L. Yan, "Multiple-channel plasmonic filter based on metal-insulator-metal waveguide and fractal theory," Plasmonics **12**, 1589–1594 (2017).
6. Y. M. El-Toukhy, M. Hussein, M. F. O. Hameed, and S. Obayya, "Characterization of asymmetric tapered dipole nanoantenna for energy harvesting applications," Plasmonics **13**, 503–510 (2018).
7. M. R. Pav, S. P. Hosseini, N. Granpayeh, and A. Rahimzadegan, "Applications of ultracompact aperture-coupled plasmonic slot cavity with spectrally splitting capability," J. Nanophoton. **12**, 016010 (2018).
8. Z. I. R. Thomas and R. Kelsall, "Silicon based plasmonic coupler," Opt. Express **20**, 21520–21531 (2012).
9. Y. Liu and Y. Lia, "Plasmonic coupler for silicon-based-micro slabs to plasmonic nano-gap waveguide mode conversion enhancement," J. Lightwave Technol. **31**, 1708–1712 (2013).
10. G. Veronis and S. Fan, "Theoretical investigation of compact couplers between dielectric slab waveguides and two-dimensional metal-dielectric-metal waveguides," Opt. Express **15**, 1–3 (2007).
11. R. A. Wahsheh, Z. Lu, and M. A. G. Abushagur, "Efficient couplers and splitters from dielectric waveguides to plasmonic waveguides," in *Frontiers in Optics*, OSA Technical Digest (CD) (Optical Society of America, 2008), paper FThS4.
12. R. A. Wahsheh, Z. Lu, and M. A. Abushagur, "Nanoplasmonic couplers and splitters," Opt. Express **17**, 19033–19040 (2009).
13. G. Veronis and S. Fan, "Bends and splitters in metal-dielectric-metal subwavelength plasmonic waveguides," Appl. Phys. Lett. **87**, 131102 (2008).
14. P. Ginzburg and M. Orenstein, "Plasmonic transmission lines: from micro to nano scale with λ/4 impedance matching," Opt. Express **15**, 6762–6767 (2007).
15. M. B. Heydari, M. Asgari, and N. Jafari, "Novel analytical model for nano-coupler between metal-insulator–metal plasmonic and dielectric slab waveguides," Opt. Quantum Electron. **50**, 432 (2018).
16. A. M. Said, A. Heikal, N. F. Areed, and S. Obayya, "Why do field-based methods fail to model plasmonics?" IEEE Photon. J. **8**, 1–13 (2016).
17. R. Yang, R. A. Wahsheh, Z. Lu, and M. A. Abushagur, "Efficient light coupling between dielectric slot waveguide and plasmonic slot waveguide," Opt. Lett. **35**, 649–651 (2010).
18. K. S. Atia, A. Heikal, and S. Obayya, "Analysis of plasmonic couplers using finite element frequency domain," in *31st International Review of Progress in Applied Computational Electromagnetics (ACES)* (IEEE, 2015), pp. 1–2.
19. S. Ramo, J. R. Whinnery, and T. Van Duzer, *Fields and Waves in Communication Electronics* (Wiley, 2008).
20. S. Orfanidis, "Electromagnetic waves and antenna," 2003, https://www.ece.rutgers.edu/~orfanidi/ewa/.
21. D. M. Pozar, *Microwave Engineering* (Wiley, 2009).
22. D. Smith, E. Shiles, M. Inokuti, and E. Palik, "Handbook of optical constants of solids," Handb. Opt. Constants Solids **1**, 369–406 (1985).